CHAPTER- III

Room Temperature Structural Studies Using Laboratory Source X-ray Powder Diffraction Data

3.1 Introduction

As discussed in chapter I, the structure of $BiFeO_3$ (BF) is rhombohedral in the R3c space group with $a^-a^-a^-$ tilt system [Jacobson et al. (1975); Fischer et al. (1980); Kubel (1990); Sosnowska et al. (2002)]. The structure of $Pb(Fe_{0.5}Nb_{0.5})O_3$ (PFN) was also regarded as rhombohedral in R3m space group in early literature [Plantov et al. (1970), Mabud (1984), Ivanov et al. (2000)] but it is now known to be monoclinic in the Cm space group [Bonny et al. (1997), and Lampis et al. (1999), Singh et al. (2007)]. Very little work has been reported on the structure of the $(BiFeO_3)_{1-x}(PbFe_{0.5}Nb_{0.5}O_3)_x$ (BF-xPFN) solid solutions. The important published research work related with the structure of the BF-xPFN solid solutions is summarized in the following. (i) It was reported that the structure of BF-xPFN solid solution for the composition range $0 \leq x \leq 0.30$ is identical with that of $BiFeO_3$, while for the compositions $0.40 \leq x \leq 0.80$, the structure is cubic [Buhrer, (1962)]. But the author's report is silent about the structures of BF-xPFN for the composition range $0.30 < x < 0.40$ and $0.80 < x < 1.0$. (ii) The presence of a broad morphotropic phase boundary (MPB) region across which structure change occurs as a function of composition at a fixed temperature was reported in the BF-xPFN solid solutions by Zhdanova (1965) using dilatometric study for the composition region $0.25 < x < 0.35$. (iii) The solid solutions containing 60% $BiFeO_3$ was reported to possess tetragonal structure which exhibits two phase transitions at $T_N \sim 393$ K and $T_C \sim 653$ K [Buhrer, (1962)]. (iv) In another work, the room temperature structure of the BF-0.8PFN composition was reported to be pseudocubic [Bhat et al. (1974)]. More recently, Paik et al. (2009) have reported

the long range ordered (LRO) normal ferroelectric domains in $Bi_{0.9}La_{0.1}FeO_3$ (BLF) while short range ordered (SRO) mottled polar domains of nanoscale order in $0.5(Bi_{0.9}La_{0.1})FeO_3$-$0.5Pb(Fe_{0.5}Nb_{0.5})O_3$ (0.5BLF-0.5PFN) using transmission electron microscopy (TEM).

The literature survey thus reveals lack of systematic crystallographic study on BF-xPFN solid solutions. No attempt has been made to refine the crystal structure using Rietveld technique. This will enable us to correlate the structural parameter with ferroic properties. In addition, there are several open questions that should be resolved such as: (i) Is there an MPB region in the phase diagram of the BF-xPFN? (ii) If yes, then what is the space group of the two phases stable in the MPB region? (iii) What is the stability field of the two end members with R3c and Cm space groups? (iv) The compositions in the range $0.40 \leq x \leq 0.80$ are reported to be cubic but show broad peak in their $\varepsilon'(T)$ plot and also *P*-*E* loops like ferroelectrics. It raises questions about their actual crystal symmetry as centrosymmetric cubic ($Pm\bar{3}m$ space group) cannot exhibit ferroelectricity. There, detailed crystallographic studies are required for establishing the temperature-composition phase diagram of $(BiFeO_3)_{1-x}(PbFe_{0.5}Nb_{0.5}O_3)_x$ at room temperature.

The present chapter and the next chapter, reports the results of a comprehensive study of the room temperature crystal structure of BF-xPFN solid solutions in the entire composition region ($0 \leq x \leq 0.96$) using laboratory source and synchrotron source based x-ray powder diffraction data.

3.2 Experimental

The different compositions of BF-xPFN samples were synthesized by the methods discussed in chapter II. The sintered pellets of different compositions were crushed using an agate mortar and pestle into fine powders. The properly crushed powders were annealed at 773 K for 12 hours to remove strains introduced during the crushing. The annealed powders were used to record the x-ray powder diffraction patterns using an 18 kW rotating anode (Cu) based Rigaku (D/Max-2500/PC series) powder x-ray diffractometer operating in the Bragg-Brentano geometry and fitted with a curved crystal monochromator in the diffracted beam. The data was recorded in the 2θ range of 20° to 120° at a step of 0.02°. A brief introduction to the Rietveld refinement technique is also included in this chapter.

3.3 Introduction to Rietveld refinement method

Rietveld technique is a computer based analytical procedure which utilizes the full information content of the powder diffraction pattern [Rietveld (1967) and (1969)]. It is a least-squares refinements method in which the refinement is carried out until the best fit is obtained between the entire observed powder diffraction pattern taken as a whole and the entire calculated pattern based on the simultaneously refined parameters of structural model used, diffraction optics, instrumental factors, and other specimen characteristics (e. g. texture etc) [Young, 1996].

The quantity minimized in the least-squares refinement is the residual, S_y [Rietveld (1967) & (1969), Young (1996)] which can be defined as

$$S_y = \sum_i w_i (y_{oi} - y_{ci})^2 \qquad (3.1)$$

where $w_i = 1/y_{oi}$,

y_{oi} = observed intensity at the i^{th} step,

y_{ci} = calculated intensity at the i^{th} step, and the sum is overall data points.

The background contribution to intensity of the powder diffraction pattern modeled using the linear interpolation between operator-selected points in the pattern or using sixth order polynomial function.

For the modeling of the peak shape pseudo-voigt (pV) peak profile function used, which is the mixture of the Lorentzian (L) and Gaussian (G) functions and can be defined as

$$pV = \eta L + (1-\eta)G \qquad (3.5)$$

where η is the mixing parameter [Young (1996)]. For angle dispersive data, the dependence of the breadth H of the reflection profiles measured as full width at half maximum (FWHM) has been modeled as [Caglioti et al. (1958)]

$$H^2 = U \tan^2\theta + V \tan\theta + W \qquad (3.6)$$

where U, V and W are the refinable parameters.

The most commonly used R-factors which decide the quality of fit is given below

(i) R-structure factor is defined as

$$R_F = \sum |(I_K(obs))^{1/2} - (I_K(cal)^{1/2})| / \sum (I_K(obs))^{1/2}$$

(ii) R-Bragg factor is defined as $R_B = \sum |I_K(obs) - I_K(cal)| / \sum I_K(obs)$

(iii) R-pattern is defined as $R_P = \sum |y_{oi}(obs) - y_{ci}(cal)| / \sum y_{oi}(obs)$

(iv) R-weighted pattern is defined as

$$R_{wp} = \left\{ \sum w_i (y_i(obs) - y_i(cal))^2 \right\}^{1/2} / \left(\sum w_i (y_i(obs))^2 \right)^{1/2}$$

(v) R-expected is defined as $R_e = \left\{ (n-p) / \sum_{i=1}^{n} w_i y_i^{\,2} \right\}^{1/2}$

Here I_K is the intensity assigned to the K^{th} Bragg reflection at the end of the refinement cycles.

(vi) The goodness of fit indicator S is defined as

$S = [R_{wp}/R_e] = [S_y/(N-P)]^{1/2}$

The goodness of fit of the system is also represented by an indicator called χ^2 and expressed as $\chi^2 = S^2 = [R_{wp}/R_e]^2 = [S_y/(N-P)]$

(vii) The Durbin-Watson statistics is defined as

'd' = $\sum_{i=2}^{N} (\Delta y_i - \Delta y_{i=N})^2 / \sum_{i=1}^{N} \Delta y_i^{\,2}$ where $\Delta y_i = y_{oi} - y_{ci}$

3.4 Rietveld refinement details of BF-xPFN

Rietveld refinements were carried out using the FULLPROF package [Carvajal (2010)]. The Wyckoff positions and the asymmetric unit for the various space groups used during the Rietveld refinements of different crystallographic phases of BF-xPFN system in the present work are given below:

(i) For the rhombohedral phase with R3m space group, we have used hexagonal axes with lattice parameters $a_H \approx b_H \approx 2^{1/2} a_R$ and $c_H \approx 3^{1/2}\, a_R$, where a_R corresponds to the rhombohedral cell parameter. There are three ions (Bi^{3+}/ Pb^{2+}, Fe^{3+}/Nb^{5+} and O^{2-}) in the asymmetric unit of the rhombohedral phase of which Bi^{3+}/ Pb^{2+} and Fe^{3+}/Nb^{5+} ions occupy 3(a) Wyckoff site at (0, 0, z) and O^{2-} occupies 9(b) Wyckoff site at (2x, x, 0.1666).

(ii) For the rhombohedral phase with the R3c space group also, we used hexagonal axes with lattice parameter $a_H \approx b_H \approx 2^{1/2} a_{pc}$ and $c_H \approx 2(3^{1/2})\, a_{pc}$, where a_{pc} corresponds to the primitive pc (pseudocubic cell) cell parameter. There are three

ions (Bi^{3+}/ Pb^{2+}, Fe^{3+}/Nb^{5+} and O^{2-}) in the asymmetric unit of the rhombohedral structure. The Bi^{3+}/ Pb^{2+} and Fe^{3+}/Nb^{5+} ions occupy the 6(a) Wyckoff site at (0, 0, z) while O^{2-} ions at the 18(b) Wyckoff sites at (x, y, z). The coordinates of all the atoms in the asymmetric unit cell of the R3c space group can also be written as a function of the displacement parameters s, t, d and e, as per Megaw et al. (1975): Bi^{3+}/ Pb^{2+} (0, 0, 0.25+s), Fe^{3+}/Nb^{5+} (0, 0, t), O^{2-} (0.1666-2e-2d, 0.3333-4d, 0.0833). The parameters 's' and 't' describe the polar displacement of cations Bi^{3+}/ Pb^{2+} and Fe^{3+}/Nb^{5+} along $[001]_h$. The displacement parameter 'e' of oxygen (O^{2-}) from its ideal cubic position is related to the tilt angle (ω) of antiphase rotation of the oxygen octahedra about the trigonal $[111]_{rh}$ or $[001]_h$ direction through the expression $\omega = \tan^{-1}(4e\sqrt{3})$. The parameter 'd' is related to the distortion of the BO_6 (B: Fe^{3+}/Nb^{5+}) octahedra.

(iii) For the monoclinic phase in the Cm space group, there are four ions (**(**Bi^{3+}/ Pb^{2+}, Fe^{3+}/Nb^{5+}, O_I^{2-} and O_{II}^{2-}) in the asymmetric unit with Bi^{3+}/ Pb^{2+}, Fe^{3+}/Nb^{5+} and O_I^{2-} occupy 2a Wyckoff sites at (x, 0, z) and O_{II}^{2-} occupies 4b Wyckoff sites at (x, y, z). Bi^{3+}/ Pb^{2+} were fixed at the origin (0, 0, 0).

(iv) For the cubic phase in the $Pm\bar{3}m$ space group, there are three ions (Bi^{3+}/ Pb^{2+}, Fe^{3+}/Nb^{5+} and O^{2-}) in the asymmetric unit of which Bi^{3+}/ Pb^{2+} ions occupy the 1(a) Wyckoff site at (0, 0, 0), Fe^{3+}/Nb^{5+} occupy 1b Wyckoff site at (0.5, 0.5, 0.5), and O^{2-} occupy 3(c) Wyckoff site at (0.5, 0.5, 0).

(v) For the tetragonal phase in the P4mm space group, there are four ions (Bi^{3+}/ Pb^{2+}, Fe^{3+}/Nb^{5+}, O_I^{2-} and O_{II}^{2-}) in the asymmetric unit with Bi^{3+}/ Pb^{2+} ion occupy 1(a) Wyckoff sites at (0, 0, z), Fe^{3+}/Nb^{5+} and O_I^{2-} occupy 1(b) Wyckoff sites at

(0.5, 0.5, z) and O_{II}^{2-} occupy 2(c) Wyckoff sites at (0.5, 0, z). Bi^{3+}/ Pb^{2+} were fixed at origin (0, 0, 0).

3.5 Results and discussion

3.5.1 Structural evidence for two morphotropic phase transitions

Composition induced structural phase transition at a constant temperature in solid solution system is called as morphotropic phase transition. In this section, we discuss how the rhombohedral structure of BF changes with substitution of PFN at room temperature. First of all, we present the qualitative interpretation of the x-ray powder diffraction data collected for various compositions of BF-xPFN in the composition range $0.1 \leq x \leq 1.0$. Fig. 3.1 depicts the x-ray diffraction profiles of the 222_{pc}, 400_{pc} and 440_{pc} [all indices are with respect to a doubled pseudocubic (pc) perovskite cell] reflections after stripping off the $CuK\alpha_2$ contribution. It is evident from this figure that, for the compositions with $x < 0.35$, the pseudocubic reflections 222_{pc} and 440_{pc} are doublets with weaker reflections occurring at lower 2θ angle side while the 400_{pc} reflection is a singlet. This type of peak characteristic is observed for the rhombohedral phase with R3c space group of BF. The rhombohedral splitting of the 222_{pc} and 440_{pc} reflections gradually decreases with increasing amount of $Pb(Fe_{0.5}Nb_{0.5})O_3$ doping (x). For x = 0.35 composition, one new reflection appears in the middle of the two 440_{pc} reflections. This reflection is probably due to a new phase which co-exists with the rhombohedral phase of BF-xPFN. For x = 0.36 composition, one single peak exists with nearly the same 2θ angle as for the peak position of the middle reflection of 440_{pc}, for x = 0.35 while the small tails of rhombohedral reflections remain at on the lower and higher 2θ sides. Also the 222_{pc} peak has a small peak marked with arrow at the lower 2θ

side. This situation seems to persist up to x = 0.40. For x > 0.40, a small intensity on higher 2θ side of 444_{pc} is due to incomplete removal of $K\alpha_2$ contribution. For x > 0.40, all the peaks are nearly singlet as expected for the cubic perovskite phase with $Pm\bar{3}m$ space group. The small asymmetry in 222_{pc} and weak humps near the tails of 400_{pc} and 440_{pc} are due to incomplete stripping of $K\alpha_2$. This point would become clear in the next where we present synchrotron x-ray powder diffraction (SXRD) data. The present observations suggest that there are two crystallographic phases which coexist in the composition range $0.35 \leq x < 0.40$ and the structure is cubic for $x > 0.40$. Above observations suggest that the first morphotropic transition in BF-xPFN is likely to occur around $x \sim 0.40$. The stability field of the rhombohedral and cubic phases in the present study is slightly different from that reported by Zhdanova (1965). The observation of phase coexistence suggests that the MPB in BF-xPFN is of first order type [Landau and Lifshits (1958)]. One of the main characteristics of the rhombohedral phase with R3c space group is the presence of $a^- a^- a^-$ type octahedral tilt [Glazer (1975)]. This tilt system (for details of tilt systems, please see Glazer (1975)] leads to cell doubling and gives rise to extra reflections in the x-ray diffraction patterns which are called as 'superlattice reflections'. Fig. 3.2(a) depicts the zoomed portion of the x-ray diffraction data for $0.1 \leq x \leq 0.5$ in the 2θ range 34 to 43° where one of the superlattice reflections occurs. The reflection indicated by asterisk is the strongest superlattice reflection 311_{pc} (Miller indices are with respect to doubled pseudocubic perovskite cell) resulting from the antiphase rotation of oxygen octahedra about the [111] rhombohedral axis.

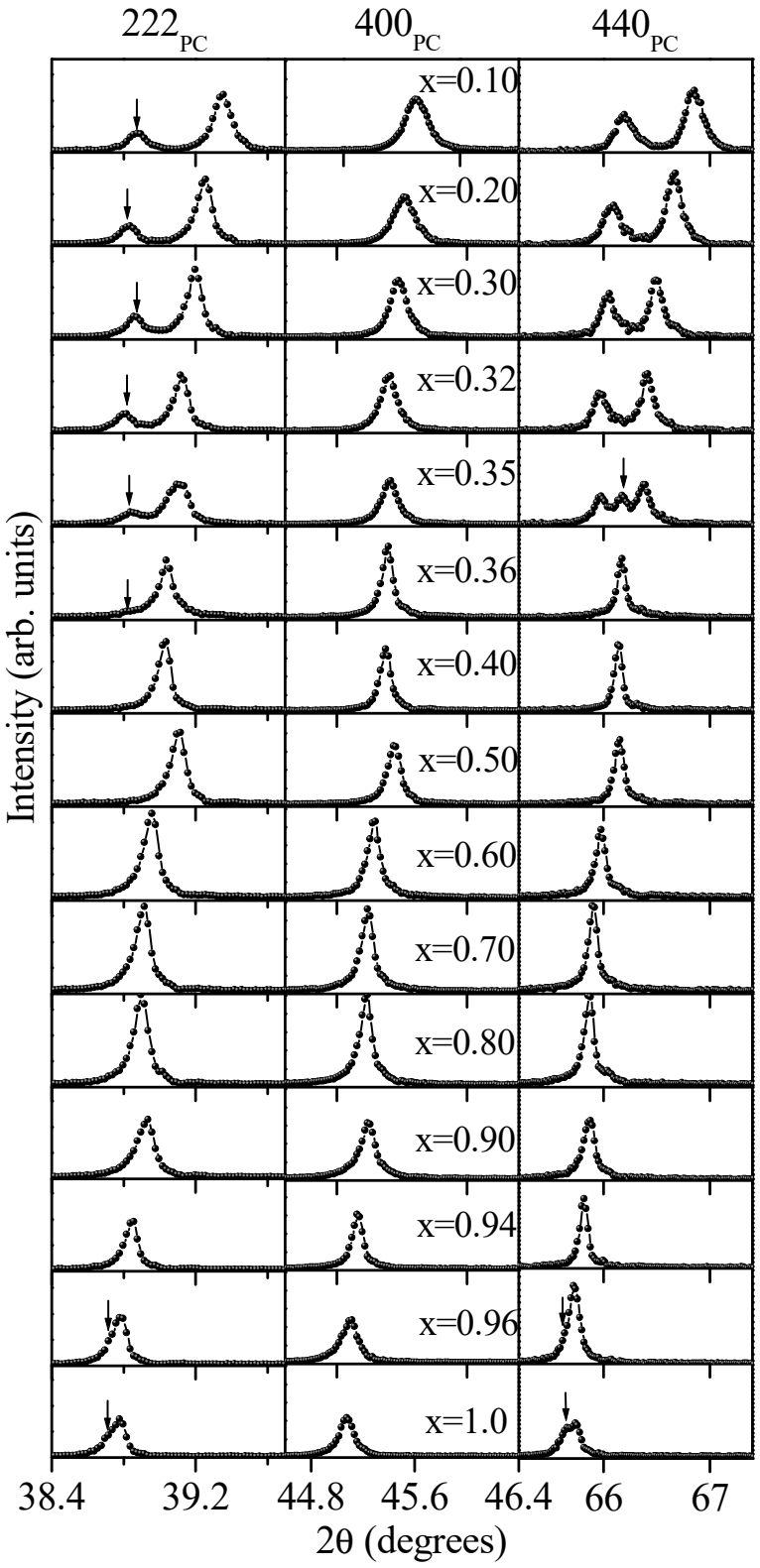

Fig. 3.1 The evolution of CuKα_2 stripped laboratory x-ray powder diffraction profiles of the 222_{pc}, 400_{pc} and 440_{pc} reflections of BF-xPFN with x.

Fig. 3.2(b) depicts the variation of integrated intensity of the strongest superlattice reflection 311_{pc} with composition. It is evident from this figure that the integrated intensity decreases linearly with increasing PFN doping (x) and becomes zero for the critical composition $x_C \approx 0.40$. The rhombohedral splitting of the pseudocubic reflections such as 222_{pc} and 440_{pc} are also disappearing completely for the x = 0.40 composition leading to singlet reflection of the cubic phase whose phase fraction seems to grow from x = 0.35 composition. The coexistence region of the two phases $0.35 \leq x < 0.40$ gives the width of the MPB as $\Delta x \approx 0.05$. Zhdanova et al. (1965) also reported $\Delta x \sim 0.05$ for BF-xPFN but in the composition range $0.25 < x < 0.35$. However, the second phase was reported to be tetragonal with P4mm space group by them. But we did not find any signature of tetragonal splitting in the two phase region and also for $x \geq 0.40$ compositions. For the tetragonal phase, the 400_{pc} and 440_{pc} peaks should be doublet while 222_{pc} a singlet which is not so for $0.40 \leq x \leq 0.90$. This will be further confined in the next chapter using SXRD data. There are no crystallographic changes for the compositions range $0.40 \leq x \leq 0.90$. All the reflections appeared to be singlet. Fig. 3.3 depicts the evolution of the 444_{pc} and 400_{pc} reflections for the composition range $0.90 \leq x \leq 1.0$ towards the PFN end. The 444_{pc} and 400_{pc} pseudocubic reflections are very broad for x = 0.90 but FWHM ratio of $(400/444_{pc})$ is same within standard deviation. The large peak broadening of 444_{pc} and 400_{pc} reflections for x = 0.90 is likely to be due to the presence of local disorder in the sample as discussed in the next chapter. The 444_{pc} reflection for x =0.94, 0.96 and 1.0 is not a singlet while 440_{pc} seems to be singlet.

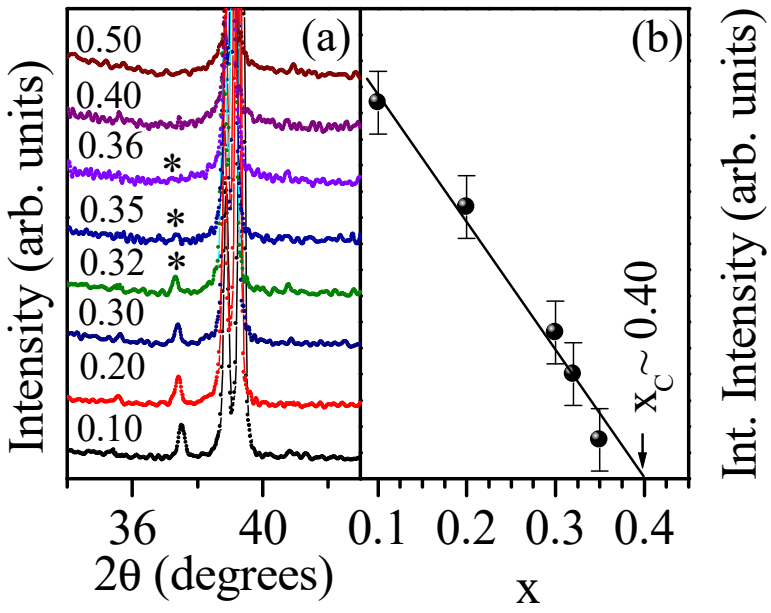

Fig. 3.2 Composition variation of (a) x-ray diffraction pattern in the selected 2θ range 34 to 43° of BF-xPFN for $0.10 \leq x \leq 0.50$, (b) integrated intensity of the 311_{pc} superlattice reflection for $0.10 \leq x \leq 0.35$. Asterisks in (a) indicate the presence of 311_{pc} superlattice reflections, while the arrow in (b) indicates the MPB composition at $x_C \sim 0.40$.

This is usually the case for rhombohedral R3m space group. But if there is any monoclinic distortion present, then FWHM ratio of 400_{pc} to 444_{pc} should be greater than 1 [Singh et al. (2007)]. Figs. 3.3(c- f) depict the deconvolution results (solid lines) of 444_{pc} and 400_{pc} reflections for the x =0.94 and 0.96 compositions and it is found that FWHM (full width at half maximum) of 400_{pc} reflection is ~ 1.1 and 1.4 times larger than FWHM of the 444_{pc} reflection. This deviation from 1.0 is the characteristic of the monoclinic phases in similar perovskites [Ragini et al. (2002), Singh et al. (2008)]. Fig. 3.3(g, h) shows the deconvolution results for 444_{pc} and 400_{pc} reflections of PFN. The ratio of the FWHM of 400_{pc} to 444_{pc} is ~

1.5, which is consistent with the short range ordered monoclinic character of the PFN reported in the literature [Bonny et al. (1997), Lampis et al. (1999), Singh et al. (2007A)].

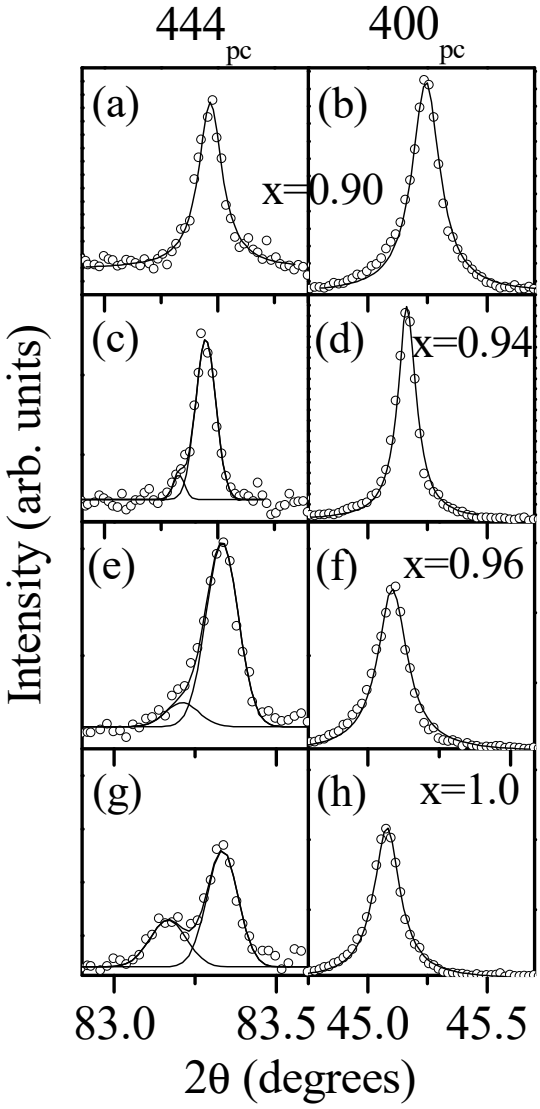

Fig. 3.3 Deconvoluted and zoomed 444_{pc} and 400_{pc} peak profiles (a - h) for x = 0.90, 0.94, 0.96 and 1.0. The open circles are the experimentally observed data points while the solid line represents the least- square fitting peak.

Based on the above qualitative discussion, we could divide the stability regions of different crystallographic phases of BF-xPFN into four groups (i) In the composition range $0.10 \leq x \leq 0.32$, the crystal structure at room temperature is

expected to be rhombohedral with R3c space group. (ii) In the composition region $0.32 < x < 0.40$, the R3c phase coexists with the cubic $Pm\bar{3}m$ phase and the structure becomes cubic at x_c=0.40. This gives the width of the MPB region as $\Delta x \approx 0.06$. Thus MPB occurs at x_c=0.40. (iii) In composition region $0.40 \leq x \leq 0.90$ the room temperature crystal structure is cubic in the $Pm\bar{3}m$ space group. (iv) There is a second MPB at $x \approx 0.90$ composition as the PFN like structure seems to exist in the composition range $0.90 < x \leq 1.0$. To provide quantitative confirmation of above structural models, we now proceed to present the Rietveld refinement results. We illustrate our findings using four representative compositions, eventhough Rietveld refinements were carried for all the compositions.

3.5.2 Rietveld refinement of the structure of BF-xPFN for $0.1 \leq x \leq 0.32$

As discussed in the previous section, the x-ray diffraction profiles of 222_{pc}, 400_{pc} and 440_{pc} pseudocubic reflections for the composition range $x \leq 0.32$ show identical features like those expected for undoped $BiFeO_3$ including the presence of the characteristic superlattice reflection 311_{pc}. Therefore, rhombohedral phase with R3c space group of $BiFeO_3$ was used for the Rietveld refinements for all the compositions of BF-xPFN with $x \leq 0.32$. Initially, the unit cell parameters and positional coordinates of $BiFeO_3$ were taken for the Rietveld refinement of the BF-xPFN for $x \leq 0.32$. The positional coordinates of all the atoms in the asymmetric unit were considered in the Megaw and Darlington coordinate system [Megaw and Darlington (1975)] as discussed in section 3.4. Fig. 3.4 depicts the Rietveld refinement fit for the BF-0.3PFN composition which is one of the selected representative compositions for $0 \leq x \leq 0.32$ range.

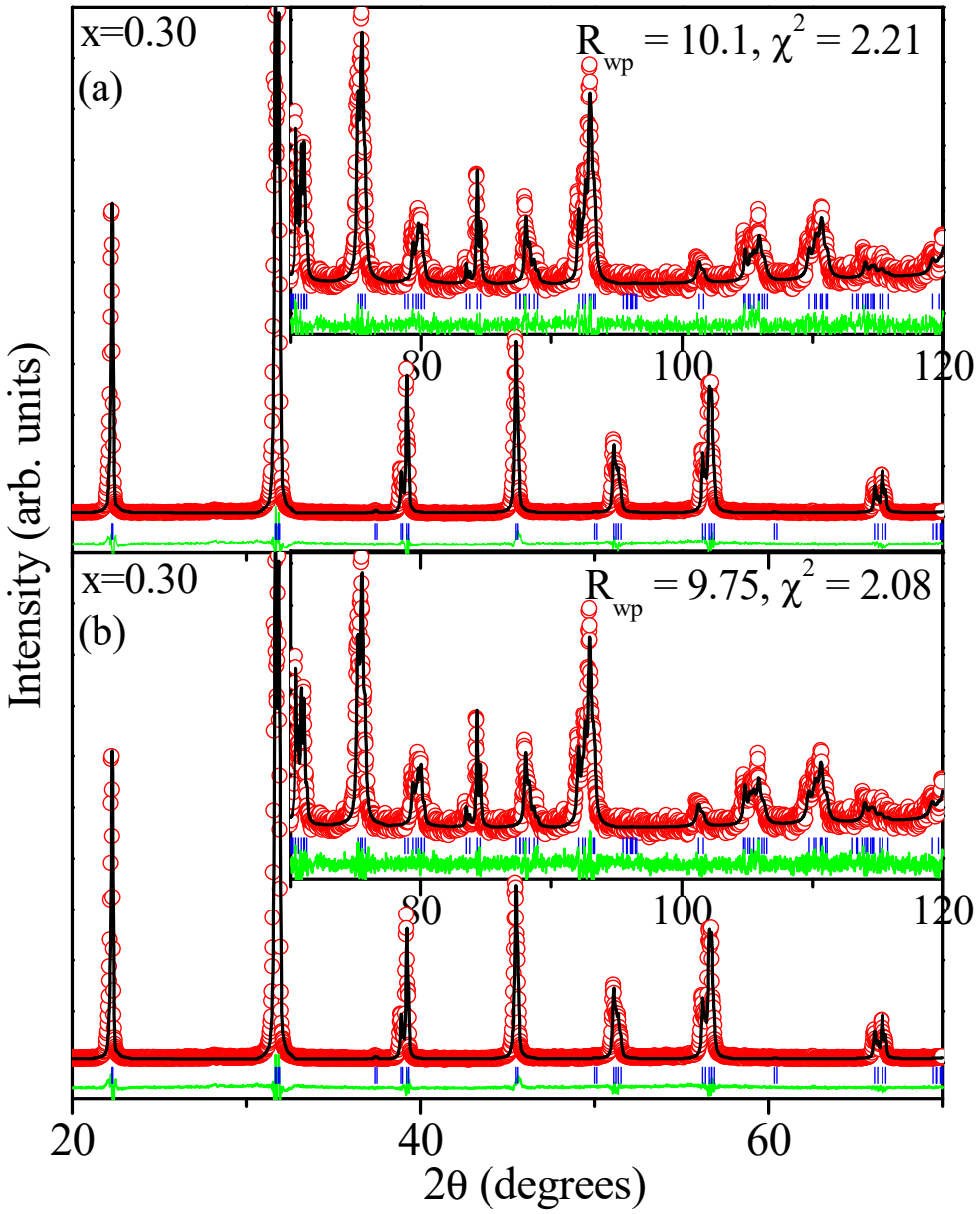

Fig. 3.4 The observed (dots), calculated (solid line) and difference profiles (bottom solid line) obtained by Rietveld analysis by using R3c space group and (a) isotropic thermal parameter (b) anisotropic thermal parameter for x = 0.30. The vertical tick marks above the difference profile correspond to the positions of the Braggs reflections. The inset indicates the zoomed portion in the 70-120° 2θ range.

The Rietveld refinement is quite good as can be seen from the fit between the observed and calculated profiles. However the isotropic thermal parameters for the

A-site and O-site ions are found to be significantly high for x = 0.30 and 0.32. Therefore, anisotropic thermal parameters were used for the Rietveld refinement which decreased the χ^2 and improved the fits as shown in Fig. 3.4 (b). The refined structural parameters are given in Table 3.1 for the compositions in the range $0.1 \leq x \leq 0.32$ at room temperature.

3.5.3 Rietveld refinement for the MPB region of BF-xPFN with $0.32 < x < 0.40$

Based on our qualitative discussion on the evolution of the x-ray diffraction profiles with change of composition, two crystallographic phases coexist in the compositions range $0.32 < x < 0.40$. Since the superlattice reflections 311pc, which is the characteristics of the R3c phase persists, in the two phase region can be seen in Fig. 3.2, one of the phases is initially considered as R3c. The second phase might be considered as tetragonal with P4mm space group based on the earlier reports [Buhrer (1962)] or $Pm\bar{3}m$ space group based on the singlet nature of the x-ray diffraction profiles in the present study and the next chapter (Fig. 4.1) for $x \geq 0.40$. Two structural models R3c+ P4mm and R3c+ $Pm\bar{3}m$ were used for the Rietveld refinement of the x-ray diffraction patterns in the composition range $0.32 < x < 0.40$. The Rietveld fit for the BF-0.35PFN compositions by using both the structural model are given in the Fig. 3.5. The fits between the observed and calculated data are satisfactory for both the structural models. The refined structural parameters of tetragonal phase with P4mm space group found to be same as for cubic phase within standard deviation obtained from the Rietveld refinement by using R3c+ P4mm and R3c+ $Pm\bar{3}m$ structural model, respectively. The isotropic thermal parameters were used for both the structural model. The

isotropic thermal parameter for Bi^{3+}/Pb^{2+} and O^{2-} is quite high for the $Pm\bar{3}m$ phase in comparison with that found for P4mm phase.

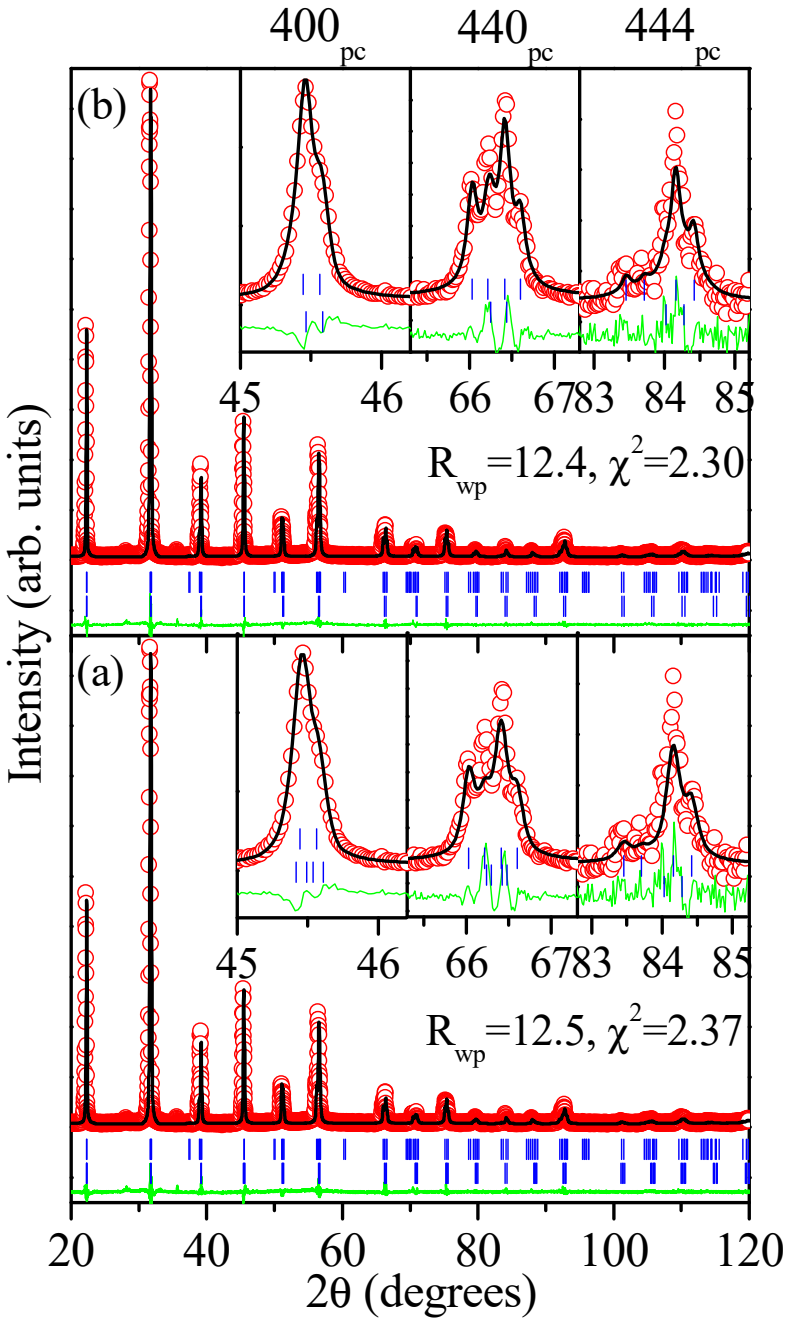

Fig. 3.5 The observed (dots), calculated (solid line) and difference profiles (bottom solid line) obtained by Rietveld analysis by using (a) R3c+ P4mm and (b) R3c+ $Pm\bar{3}m$ space group for x = 0.35. The vertical tick marks above the difference profile correspond to the positions of the Braggs reflections. The inset indicates the zoomed portion in the 70-120° 2θ range.

Since both the structural models R3c+ P4mm and R3c+ $Pm\bar{3}m$ give same structural parameters within standard deviation, it is very difficult to choose which one is correct model by using laboratory x-ray diffraction data. The refined coordinates and lattice parameters for x = 0.35 compositions are given in the Table.3.1 for the $Pm\bar{3}m$ space group as it has got lower number of refinable parameters than the tetragonal P4mm space group and gives nearly comparable R_{wp}, χ^2 and quality of fit.

3.5.4 Rietveld refinement of BF-xPFN for $0.40 \leq x \leq 0.90$

The x-ray diffraction data in the composition range $0.40 \leq x \leq 0.90$ reveals that superlattice reflection and rhombohedral splittings have completely disappeared. All the reflections of the x-ray diffraction pattern recorded in this composition range are singlet. Therefore, $Pm\bar{3}m$ structural modal was used for the Rietveld refinement of BF-0.4PFN. Buhrer (1962) reported that a tetragonal phase with P4mm space group for BF-0.4PFN solid solution. Therefore, we also considered the tetragonal phase with P4mm space group for the refinement. All the peaks were indexed adequately by both tetragonal and cubic symmetry. The Rietveld refinement fits for BF-0.4PFN composition by using P4mm and $Pm\bar{3}m$ space group is shown in the Fig. 3.6. The refined lattice parameters of tetragonal phase are equal with the cubic phase within the standard deviation, while the positional coordinates differ slightly from their ideal cubic position. The Δz shift in the refined positional coordinates from the ideal cubic position for Fe^{3+}/Nb^{5+}, O_I^{2-} and O_{II}^{2-} in the tetragonal model is found to be 0.02(1), 0.04(2) and 0.15(7) respectively. We observed very high value of isotropic thermal parameters for the Bi^{3+}/Pb^{2+} and O^{2-} ions when the structural model was considered to be cubic while

when we assumed tetragonal model with P4mm space group the very large value of isotropic thermal parameter was found only for Bi^{3+}/Pb^{2+}. Surprisingly, the R_{wp} and χ^2 are comparable for both the models, eventhough the tetragonal model has more number of refinable parameters following crystallographic convention of getting the best fit with minimum number of refinable parameters, and we assign $Pm\bar{3}m$ average structure to this composition. The isotropic thermal parameter for Fe^{3+}/Nb^{5+} ions is acceptable at room temperature for both the models. The isotropic thermal parameters for Bi^{3+}/Pb^{2+} and O^{2-} ions are found to be quite high for all other compositions in the range $0.40 \leq x \leq 0.90$ as in case of BF-0.4PFN. Therefore, anisotropic thermal parameters were used for Bi^{3+}/Pb^{2+} and O^{2-} ions during the refinement. All other compositions of the present phase region are refined well by considering the $Pm\bar{3}m$ model. The unusually large values of isotropic thermal parameters for Bi^{3+}/Pb^{2+} and O^{2-} ions indicate that these ions are locally displaced from their ideal cubic positions. It seems that the average crystal structure of BF-xPFN for $0.40 \leq x \leq 0.90$ is cubic with local disorder. We shall revisit the tetragonal P4mm model and the cubic $Pm\bar{3}m$ model with local disorder with high 'q' data obtained from synchrotron source in the next chapter where we shall confirm the average cubic structure model with local disorder convincingly. The refined lattice parameters, isotropic thermal parameters and statistical parameters are given in the Table 3.1 for the composition range 0.40 to 0.90 using $Pm\bar{3}m$ cubic space group.

Table 3.1 Rietveld refinement results of x-ray diffraction data collected on BF-xPFN solid solution for different values of x.

x	0.1	0.2	0.3	0.32	0.35	0.4	0.5	0.6	0.7	0.8	0.9	0.94	0.96
Space Group	R3c	R3c	R3c	R3c	R3c+Pm-3m	Pm-3m	Pm-3m	Pm-3m	Pm-3m	Pm-3m	Pm-3m	Cm	Cm
a(Å)	5.5888(8)	5.6014(4)	5.6182(3)	5.6203(1)	5.6259, 3.999	3.9905(6)	3.9972(8)	4.0004(5)	4.0041(5)	4.0072(4)	4.0094(7)	5.6717(5)	5.6725(5)
b(Å)	5.5888(8)	5.6014(4)	5.6182(3)	5.6203(1)	5.6259, 3.999	3.9905(6)	3.9972(8)	4.0004(5)	4.0041(5)	4.0072(4)	4.0094(7)	5.6699(5)	5.6708(4)
c(Å)	13.868(8)	13.8817(3)	13.8878(5)	13.888(6)	13.8871,3.999	3.9905(6)	3.9972(80	4.0004(5)	4.0041(5)	4.0072(4)	4.0094(7)	4.0132(6)	4.0159(4)
β												90.025(1)	90.038(2)
(Bi/ Pb)x	0	0	0	0	0, 0	0	0	0	0	0	0	0	0
(Bi/ Pb)y	0	0	0	0	0, 0	0	0	0	0	0	0	0	0
(Bi/ Pb)z	0.2976(2)	0.2922(3)	0.2879(5)	0.285(4)	0.283(3), 0	0	0	0	0	0	0	0	0
(Fe/Nb)x	0	0	0	0	0, 0.50	0.5	0.5	0.5	0.5	0.5	0.5	0.493(5)	0.501(3)
(Fe/Nb)y	0	0	0	0	0, 0.50	0.5	0.5	0.5	0.5	0.5	0.5	0.0	0.0
(Fe/Nb)z	0.0199(5)	0.0169(5)	0.0136(5)	0.0129(5)	0.0118, 0.50	0.5	0.5	0.5	0.5	0.5	0.5	0.471(3)	0.470(2)
(O_I)x	0.252(4)	0.228(2)	0.209(6)	0.206(4)	0.2025, 0.50	0.5	0.5	0.5	0.5	0.5	0.5	0.514(4)	0.504(3)
(O_I)y	0.377(4)	0.347(3)	0.343(7)	0.341(9)	0.3404, 0.50	0.5	0.5	0.5	0.5	0.5	0.5	0.0	0.0
(O_I)z	0.08333	0.08333	0.08333	0.08333	0.0833, 0.00	0	0	0	0	0	0	0.172(1)	0.074(3)
(O_{II})x												0.275(2)	0.245(3)
(O_{II})y												0.236(4)	0.248(2)
(O_{II})z												0.440(2)	0.435(3)
B_{iso}(Å^2)Bi/Pb	0.85(3)	0.99(2)	2.42(3)	2.76(4)	3.38(5), 2.2(3)	4.83(8)	4.73(6)	4.61(2)	4.49(6)	3.86(4)	3.06(4)	2.45(3)	2.02(2)
B_{iso}(Å^2)Fe/Nb	0.20(3)	0.40(4)	0.51(2)	0.70(3)	1.10(2),0.19(2)	1.45(3)	1.21(4)	0.89(5)	0.74(2)	0.67(5)	0.49(5)	1.12(2)	1.2(3)
B_{iso}(Å^2) O_I	1.10(4)	1.14(3)	2.21(5)	3.33(5)	3.6(4), 2.57(2)	4.3(5)	3.86(3)	3.77(3)	3.56(2)	3.15(2)	2.0(2)	2.03(4)	1.9(3)
B_{iso}(Å^2) O_{II}												1.5(3)	1.2(2)
R_{WP}	14.8	14.3	9.75	12.5	12.4	11.0	14.9	13.6	13.6	13.7	13.2	16.8	14.0
χ^2	4.13	1.47	2.08	2.58	2.30	2.04	3.93	3.92	3.98	2.8	2.72	4.00	2.63

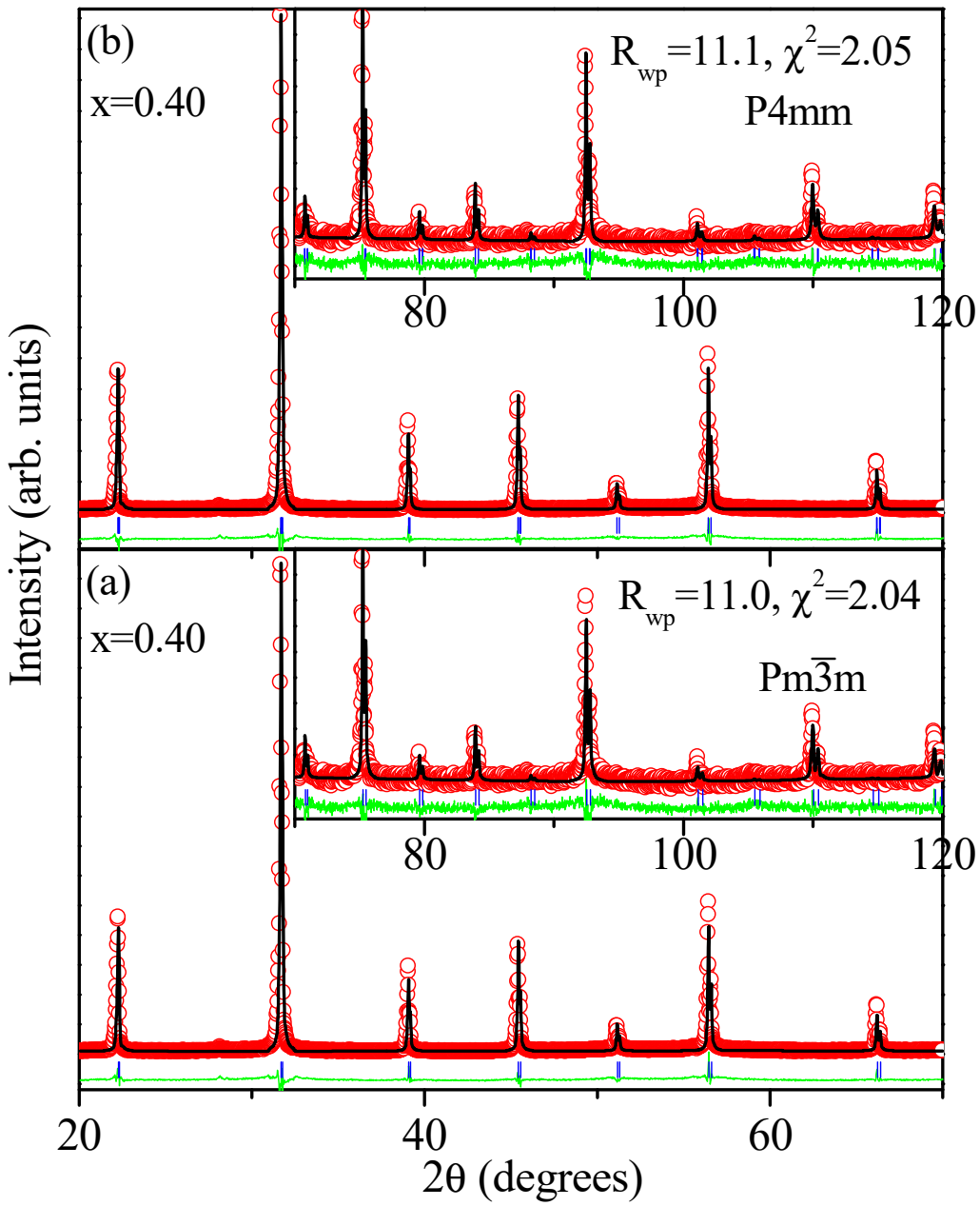

Fig. 3.6 The observed (dots), calculated (solid line) and difference profiles (bottom solid line) obtained by Rietveld analysis by using (a) $Pm\bar{3}m$ and (b) P4mm space group for x = 0.40. The vertical tick marks above the difference profile correspond to the positions of the Braggs reflections. The inset indicates the zoomed portion in the 70-120° 2θ range. Note the diffuse scattering at the tails of various peaks which cannot be accounted by either of the two models.

3.5.5 Rietveld refinement of monoclinic phase with Cm space group of BF-xPFN for the $0.90 < x \leq 1.0$

The evolution of x-ray powder diffraction profiles shown in Fig. 4.1 reveals that for x=0.94 and 0.96 the hhh_{pc} reflections are broadened on the lower 2θ angle side which can be deconvoluted into two peaks. If the ratio of the FWHM for $h00_{pc}$ type reflection nearest to hhh_{pc} type reflection is nearly 1, then the symmetry might be R3m. where as if the ratio is greater than 1, then there is a possibility for monoclinic Cm space group similar to that reported for PFN [Bonny et al. (1997), Lampis et al. (2002)]. In the present case, we have found that ratio of FWHM of 400 and 444 is greater than 1 for $x > 0.90$ compositions. Therefore, we refined crystal structure of BF-xPFN in the composition region $0.90 \leq x \leq 1.0$ by considering monoclinic structure with Cm space group. Fig. 3.7 depicts Rietveld fit for BF-0.96PFN using Cm space group. The Rietveld refinement fit between the observed and calculated profiles is may be considered satisfactory but is not very good. The mismatch between observed and calculated peaks profiles for some reflections could be seen in the inset of Fig. 3.7. We shall discuss this issue in the next chapter by using high resolution synchrotron x-ray diffraction data. The refined value of the lattice parameter, positional coordinates and thermal parameters using Cm space group, however, are given in Table 3.1.

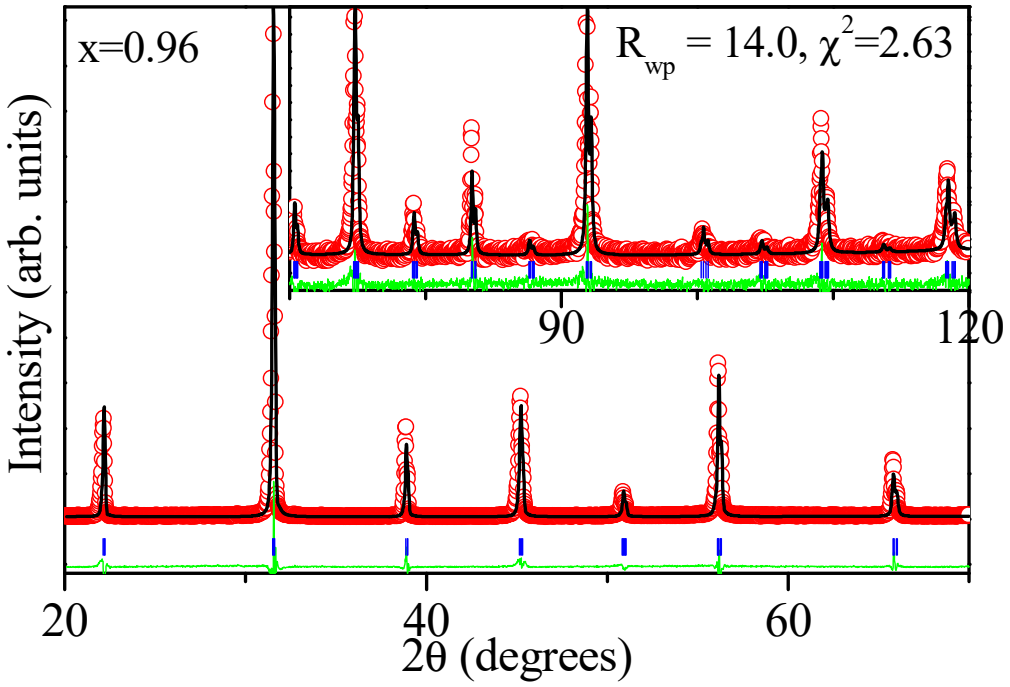

Fig. 3.7 The observed (dots), calculated (solid line) and difference profiles (bottom solid line) obtained by Rietveld analysis by using Cm space group for x = 0.96. The vertical tick marks above the difference profile correspond to the positions of Braggs reflections. The inset indicates zoomed portion in the 70-120° 2θ range.

3.5.6 Variation of structural parameters with compositions

The pseudocubic lattice parameters a_{pc} and c_{pc} for rhombohedral cell is obtained by using $a_{pc} \approx a_H/\sqrt{2}$ and $c_{pc} \approx c_H/2\sqrt{3}$ relationship where a_H and c_H are lattice parameters of the rhombohedral cell in hexagonal setting while pseudocubic cell parameters for the monoclinic phase is obtained by using $a_m \approx A_m/\sqrt{2}$, $b_m \approx B_m/\sqrt{2}$ and $c_m \approx C_m$, relationship where A_m, B_m and C_m are lattice parameters of monoclinic cell (b-axis setting), whereas a_m, b_m, c_m are the pseudocubic cell parameters. Fig. 3.8(a) depicts variation of pseudocubic unit cell lattice parameters of BF-xPFN with x in the composition range $0 \leq x \leq 1.0$. The structural

parameters for pure BF (x = 0) and pure PFN (x = 1.0) were taken from the literature [Reyes et al. (2007), Singh et al. (2007A)]. The pseudocubic lattice parameter a_{pc} in the rhombohedral phase region increases with x and approaches the lattice parameter of cubic phase i.e. a_{pc}= c for x_C = 0.40 while the other lattice parameter c_{pc} initially increases and attains a maximum value for the x = 0.32 and then sharply decreases to the lattice parameter for the cubic phase at x_C = 0.40. The maximum value of c_{pc} for x= 0.32 means that elongation of unit cell along $[111]_{pc}$ in rhombohedral phase is maximum for this composition. The rhombohedral to cubic phase transition occurs over a composition range $0.32 < x < 0.40$ where both the phases coexist at the critical composition $x_C \approx 0.40$ the structure becomes cubic. The unit cell parameter of cubic phase corresponding to the compositions in the two phase region increases linearly with x. The lattice parameter corresponding to the cubic phase in the composition range $0.40 \leq x \leq 0.90$ also increases with x. The M_A-type ($a_m \approx b_m < c_m$) monoclinic phase [Vanderbilt and Cohen (2001)] with Cm space group persists in the composition region $0.9 < x \leq 0.96$. The monoclinic cell parameters a_m and b_m increase with x while c_m initially increases with x up to x = 0.96 and then decreases with increasing x as can be seen more clearly in the inset. Fig. 3.8(b) depicts variation of the unit cell volume with x. The unit cell volume (pseudocubic) for the rhombohedral phase obtained by using the relation $V \sim a_H^2 * c_H / 4\sqrt{3}$ increases linearly with x for the rhombohedral phase. The morphotropic phase transition occurring through phase coexistence region shows the first order character of the phase boundary (MPB). Such a phase transition is usually accompanied with the change of unit cell volume. However, the unit cell volume for two phases (R3c and $Pm\bar{3}m$) which co-exist in the two

phase region is almost the same. This suggests that the discontinuous change in the unit cell volume at the MPB may be within the standard deviation.

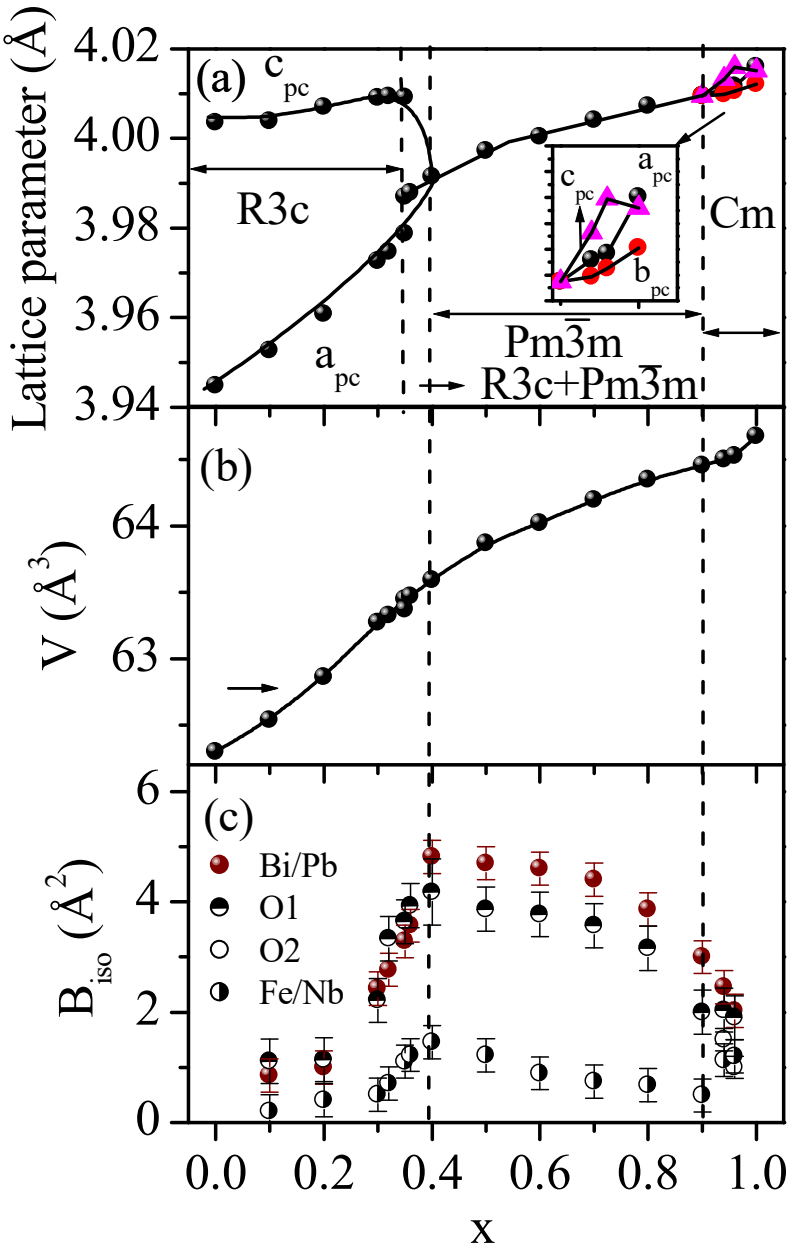

Fig. 3.8 Composition variation of (a) refined pseudocubic lattice parameter, (b) pseudocubic unit cell volume (c) isotropic thermal parameters for the Bi^{3+}/Pb^{2+}, O^{2-} and Fe^{3+}/Nb^{5+} ions.

The unit cell volume of the cubic phase of BF-xPFN for $0.40 \leq x \leq 0.90$ compositions increases slowly with x in comparison to the rhombohedral phase where the slope is high. The unit cell volume for $x > 0.90$ of the monoclinic phase

is also increases with x. The change in slope at x = 0.40 and 0.90 in the unit cell volume corresponds to the two morphotropic phase boundaries (MPBs) of the BF-xPFN system. Fig. 3.8(c) depicts the variation of isotropic thermal parameters (B_{iso}) for the Bi^{+3}/Pb^{+2}, Fe^{+3}/Nb^{+5} and O^{-2} ions with composition (x). The isotropic thermal parameter for Bi^{+3}/Pb^{+2} and O^{-2} ions increases with x in the rhombohedral phase and achieves maximum value at the first MPB at $x_C \sim 0.40$. After that it decreases slowly in the cubic phase region $0.40 \leq x \leq 0.90$. The isotropic thermal parameter for the Fe^{+3}/Nb^{+5} ions follows the same trend as for Bi^{+3}/Pb^{+2} and O^{-2} ions with x but magnitude of the thermal parameter is comparatively smaller (B_{iso} for $Fe^{+3}/Nb^{+5} \leq 1.5$ Å^2).

The enormously high values of thermal parameters for Bi^{+3}/Pb^{+2} and O^{-2} ions imply local disorder of Bi^{+3}/Pb^{+2} and O^{-2} ions which are commonly reported in most of the Pb-based perovskites like $PbZr_{1-x}Ti_xO_3$ (PZT), $Pb(Mg_{1/3}Nb_{2/3})O_3$, and $Pb(Sc_{1/2}Nb_{1/2})O_3$ systems etc [Noheda et al. (1999), Dkhil et al. (2001), Malibert et al. (1997)]. It is interesting to note that the same thermal parameters decreases significantly in the monoclinic phase region $0.90<x\leq1.0$ and attain acceptable values ≈1.0.

3.6 Summary and conclusion

Based on our qualitative and Rietveld analysis of x-ray diffraction data, the room temperature crystal structure of BF-xPFN is summarized as follows:

(i) The room temperature crystal structure of BF-xPFN in the composition range $0.1 \leq x \leq 0.32$ is identical with $BiFeO_3$. It has got rhombohedral structure with R3c space group.

(ii) A morphotropic phase transitions occurs in the composition range $0.32 < x < 0.40$ where rhombohedral and cubic phases coexist. This contradicts the previously reported coexistence region of $0.25 < x < 0.35$ by Zhdanova et al. (1965) with R3c+P4mm phase. The R3c + $Pm\bar{3}m$ structural model for phase coexistence with less number of parameters gives better fit in comparison to R3c + P4mm structural model.

(iii) The rhombohedral (R3c) to cubic ($Pm\bar{3}m$) phase transition is completed at $x_C \sim 0.40$. There is no evidence for a rhombohedral to tetragonal phase transition reported by Ismailzade et al. (1965). The cubic structural model with $Pm\bar{3}m$ space group was used for the Rietveld refinement of all the compositions in the range $0.40 \leq x \leq 0.90$. This model indexed all the reflections of the x-ray diffraction patterns. However, it gives very high values for the isotropic thermal parameters for the A-site and O-site ions. The anomalously high thermal parameters (B_{iso}) indicate the possibility for the positional disorder at A and O-sites. This issue is addressed in the next chapter.

(iv) The cubic like phase in the composition range $0.40 \leq x \leq 0.90$, transforms to Cm phase for $x > 0.90$. The x-ray diffraction patterns recorded for the composition range $0.90 < x \leq 0.96$ are refined by monoclinic phase with Cm space group.